JOURNAL OF
CHEMICAL &
ENGINEERING
DATA

ARTICLE

pubs.acs.org/jced

Relationship between Thermodynamic Data and Adsorption/Desorption Performance of Acid and Basic Dyes onto Activated Carbons

Unai Iriarte-Velasco,*[‡] Noemí Chimeno-Alanís,[†] M.P. González-Marcos,[†] and Jon I. Álvarez-Uriarte[†]

[†]Department of Chemical Engineering, Faculty of Science and Technology, University of The Basque Country, Barrio Sarriena, s/n, 48940 Leioa, Spain

[‡]Department of Chemical Engineering, Faculty of Pharmacy, University of the Basque Country, Paseo de la Universidad, 7, 01006 Vitoria, Spain

ABSTRACT: Adsorption properties of two activated carbons were investigated as a function of several operating parameters such as initial dye concentration, contact time, pH, and temperature. Adsorption/desorption performance was related to the structural and thermodynamic properties of the adsorbent. To evaluate the effect of the adsorbate an acid dye (alizarin red S, ARS) and a basic dye (methylene blue, MB) were used. Results obtained suggest that a low basicity of the adsorbent is a key factor independent of the acid or basic nature of the adsorbate. Langmuir isotherms best represent the adsorption system. Reported maximum adsorption capacities for ARS and MB were 762 $\text{mg}\cdot\text{g}^{-1}$ and 742 $\text{mg}\cdot\text{g}^{-1}$, respectively. The adsorption process followed the pseudo-first-order model. The thermodynamic parameters such as Gibbs energy ($\Delta G°$), entalphy ($\Delta H°$), and entropy ($\Delta S°$) indicate that the adsorption of the basic dye was significantly dependent on AC properties. Hydrophobic interaction played a dominant role in the adsorption of the basic dye, whereas acid dye was bound through electrostatic interaction. This coincided with the lower activation energy values reported for MB [(9.58 to 18.68) $\text{kJ}\cdot\text{mol}^{-1}$] in comparison to ARS [(23.79 to 27.67) $\text{kJ}\cdot\text{mol}^{-1}$]. Finally, for adequate desorption it is more important to enhance interaction between dye and surfactant rather than the repulsion between micelles and the adsorbent surface.

INTRODUCTION

In the last few decades, there has been a high increase in production and utilization of dyes. This has resulted in a big threat of water pollution because even at a very low concentration dyes are highly visible and may cause toxic effects in the aquatic ecosystem. It is difficult to treat dye effluents because of the negligible biodegradable nature of these compounds. There exists a wide range of treatment methods for their removal from effluents: chemical oxidation,[1] foam flotation,[2] electrolysis,[3] biodegradation,[4,5] chemical coagulation,[6] photocatalysis,[7,8] and adsorption.[9,10] All of them have advantages and disadvantages. The main advantages of adsorption as a potentially successful alternative for the removal of dyes in wastewater are the flexibility in operation, the ease of design, and the fact that adsorption does not lead to formation of harmful substances.

Abundant literature exists involving the application of adsorbents as, for example, perlite,[11] bentonite,[12] silica gels,[13] fly ash,[14] lignite,[15] peat,[16] silica,[17] and activated carbon (AC), which is regarded as one of the most effective methods, and it is therefore widely used in various industrial processes as an adsorbent.[18−20]

The adsorption process results from interactions between the carbon surface and the adsorbate. These interactions can be electrostatic or nonelectrostatic. When the adsorbate dissociates in aqueous solution, electrostatic interactions occur; the nature of these interactions, that can be attractive or repulsive, depends on the charge density of the carbon surface, on the chemical characteristics of the adsorbate, and on the ionic strength of the solution. Nonelectrostatic interactions are always attractive and can include van der Waals forces, hydrophobic interactions, and hydrogen bonding. It is known that the adsorption properties of activated charcoal depends mainly on its particle size, porosity, surface chemistry, and operational conditions such as dye concentration, pH, temperature, and flow regime.

At large scale, besides the attainment of sufficient uptake capacity and rate, an adequate treatment should also ensure minimum operational costs and disposal problems. The high cost of manufacturing of activated carbon has been traditionally a hindrance. Thus, the regeneration ability of any potential adsorbent should also be considered. Thermal regeneration is commonly used. However, it results in significant mass losses due primarily to the evaporation of moisture and the combustion of a relatively small portion of the activated carbon.[21] Chemical regeneration is an alternative to thermal treatment because it allows in situ regeneration and avoids the loss of carbon.

Though conventional activated carbon contains mostly micropores, the activated carbon produced from some raw materials has a large volume of mesopores. In this study adsorption and regeneration performance was analyzed for a wood-activated carbon having mostly mesopores and was compared to a conventional coal-based activated carbon. In this context, a cationic dye and an anionic dye were selected for the study to cover different adsorbent−adsorbate interactions. Methylene blue

Received: November 3, 2010
Accepted: March 18, 2011
Published: March 25, 2011

dx.doi.org/10.1021/je1011345 | J. Chem. Eng. Data 2011, 56, 2100–2109

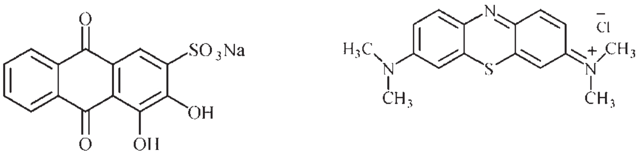
Alizarin red S Methylene blue

Figure 1. Molecular structure of ARS and MB.

Table 1. Physical and Chemical Properties of Activated Carbons

	GAC-F400	GAC-L27
origin	coal	wood
bulk density/$g \cdot mL^{-1}$	0.43	0.55
$S_{BET}/m^2 \cdot g^{-1}$	925	1345
$V_{total}/mL \cdot g^{-1}$	0.55	1.05
V_{micro} [(0.7 to 0.1) nm]/$mL \cdot g^{-1}$	0.27	0.18
$V_{supermicro}$ [(0.1 to 0.2) nm]/$mL \cdot g^{-1}$	0.17	0.23
V_{meso} [(0.2 to 0.5) nm]/$mL \cdot g^{-1}$	0.11	0.65
Av. pore size/nm	1.01	1.79
pH_{PZC}	10.2	9.5
T_{50}/K	585	596
Ash/%	7.8	6.2
acidity/$meq \cdot g^{-1}$	0.11	0.10
basicity/$meq \cdot g^{-1}$	0.25	0.10

(MB) was used as the cationic dye because it is widely used in adsorption studies.[22] Alizarin red S (ARS) was selected as the anionic dye because of its similar molecular weight to MB but different electrostatic charge. It is a widespread polluting dye whose elimination from effluents is a serious challenge.

The activated carbons were thoroughly characterized, and the adsorption performance was studied as a function of physical and chemical properties of the adsorbents and operational conditions. Kinetic and thermodynamic data were obtained. Finally, surfactant-enhanced regeneration of the exhausted carbons was evaluated.

■ EXPERIMENTAL SECTION

Adsorbates. Alizarin red S (1,2-dihydroxy-9,10-anthraquinonesulfonic acid sodium salt, ARS) is a water-soluble, widely used anthraquinone dye synthesized by sulfonation of alizarin. Anthraquinone dyes like ARS, with pK_a values of 4.5 and 11.0, are recalcitrant and durable pollutants, released especially by the textile industries to aquatic ecosystems.[4] Methylene blue (MB) is a widely used cationic dye with $pK_a > 12$. The chemical structures are shown in Figure 1. The concentration of dyes in solution was measured spectrophotometrically at a wavelength of 820 and 665 nm for MB and ARS, respectively.

Adsorbents. Two activated carbons with different textural and surface properties, Filtrasorb 400 (F-400) and Picahydro 27 (L27), were selected for this research. Physical and chemical properties of ACs are shown in Tables 1 and 2. ACs were subjected to repeated washing with water to remove dust and soluble impurities and then sieved to (0.7 to 1.0) mm.

Table 2. Elemental Analysis of Activated Carbons in Percent w/w

	C	H	N	S	Ash	O
GAC-F400	87.4	0.6	0.3	0.1	5.6	6.2
GAC-L27	92.3	0.5	0.1	0.1	6.2	0.8

Characterization of Activated Carbons. A porosimeter system (ASAP 2010, Micromeritics) was used to determine the textural properties of the washed and dried carbon samples. Prior to the measurements the samples were outgassed at 320 °C under nitrogen flow for 3 h. The total pore volume was calculated from the adsorbed volume of nitrogen gas at 77 K and near the saturation point ($P/P_o = 0.98$). Surface area was calculated from the BET method. The pore volumes were determined using density functional theory (DFT) by assuming the graphite model with slit shape geometry. Thermogravimetric analysis (TGA) was performed with a SETSYS Evolution thermal analyzer. Samples were heated under synthetic air and from room temperature up to 900 °C by using a heating rate of 5 $°C \cdot min^{-1}$. The contents of C, H, N, and S of the selected samples were measured using a CHNS-O Euro EA3000 Elemental Analyzer. The oxygen contents of samples were calculated by difference. Acidity and basicity of the carbon surface were measured from titration techniques.[23] Vials (65 mL) were filled with 0.1 g of carbon and 20 mL of 0.05 N NaOH or 0.05 N HCl. Vials without carbon and containing either acid or base were prepared as blanks. Samples and blanks were shaken at 200 rpm for 48 h at room temperature. Finally, samples were filtered (0.45 μm), and 15 mL of the solution was titrated with 0.05 N of either NaOH or HCl solution. For the determination of the pH_{PZC}, 20 mL of a $NaNO_3$ 0.1 M solution was put into several closed amber glass vials. The pH within each flask was adjusted to a value between 2 and 12 by adding 0.1 M HNO_3 or 0.1 M NaOH. Then, 0.1 g of carbon was added to each flask, and the final pH was measured after 24 h under agitation at room temperature. The pH_{PZC} is defined as the point where the curve pH_{final} vs $pH_{initial}$ shows a plateau or crosses the line $pH_{final} = pH_{initial}$. Blank tests without carbon were also prepared to eliminate the influence of CO_2 from air on pH.

Batch Adsorption. Batch adsorption experiments were done to obtain kinetic and equilibrium data. Adsorption data were determined individually for each dye–adsorbent system using the concentration-variation method. Activated carbon (0.025 g) was added to 10 mL of solution containing different concentrations of dyes. pH was set at 7.0 for all experiments except those prepared to evaluate the effect of the pH itself. The initial dye concentration was varied from (100 to 3000) $mg \cdot L^{-1}$. Adsorption solutions were sealed in corning vials and placed in a rotary shaker which was placed within a temperature controlled chamber for 24 h. The equilibrium time was determined from earlier kinetic studies. At the end of the incubation time activated carbon was separated by centrifugation at 22 °C and 4000 rpm for 10 min. The remaining dye in solution was measured by absorbance using predetermined calibration curves. The surface concentration of dyes at contact time t (q_t) was estimated from the mass balance eq 1. Solutions containing no adsorbent were used as blanks.

$$q_t = (C_o - C_t)\frac{V}{m} \tag{1}$$

where C_o and C_t are the initial and time t liquid phase concentration of the dye ($mg \cdot L^{-1}$), respectively; V is the volume of the solution (L); and m is the amount of AC used (g). 15 % of the batch experiments (randomly selected) were performed in duplicate to check for reproducibility. The measured average standard deviations were always below 10 %.

Adsorption data were fitted by nonlinear regression to the Freundlich and Langmuir isotherms, and the corresponding adsorption parameters have been calculated. The Freundlich isotherm is given by eq 2

$$q_e = K_F \cdot C_s^{1/n_F} \qquad (2)$$

where q_e is the amount adsorbed in equilibrium per unit mass of the adsorbent; C_s is the dye concentration in solution at equilibrium; and $1/n$ and K_F are constants. When the values of K_F increase, the capacity of adsorption of the adsorbent for a certain dye increases. Values in the range $0 < 1/n < 1$ represent favorable adsorption conditions. The Langmuir isotherm is given by eq 3

$$q_e = \frac{Q \cdot b \cdot C_s}{1 + b \cdot C_s} \qquad (3)$$

where Q is the monolayer capacity and b is the adsorption coefficient related to the adsorption energy.

Thermodynamic Data. Thermodynamic parameters related to the adsorption of dyes such as Gibbs energy change ($\Delta G°$), enthalpy change ($\Delta H°$), and entropy change ($\Delta S°$) were calculated using the following equations

$$\ln K_c = -\frac{\Delta H°}{RT} + \frac{\Delta S°}{R} \qquad (4)$$

$$\Delta G° = \Delta H° - T \cdot \Delta S° \qquad (5)$$

The equilibrium constant K_c of the adsorption process was calculated as the product of the Langmuir constants $Q \cdot b$ $[L \cdot g^{-1}]$.[24]

Regeneration of Activated Carbons. The effectiveness of surfactant-based regeneration was investigated. Sodium dodecyl sulfate (SDS) (M_w 288.38 Da, purity: > 96 %) was used as an anionic surfactant, and hexadecyltrimethylammonium bromide (HDTA) (M_w 364.45 Da, purity: > 98 %) was used as a cationic surfactant (Figure 2). Only when micelles are present does significant desorption of such solutes from surfaces occur. The critical micelle concentration for SDS and HDTA was reported as $2.36\ g \cdot L^{-1}$ and $0.75\ g \cdot L^{-1}$, respectively.[25] Three regeneration solutions were prepared. These included: NaOH 0.1 M, NaOH 0.1 M + $3.2\ g \cdot L^{-1}$ SDS, and NaOH 0.1 M + $1.5\ g \cdot L^{-1}$ HDTA. An amount of spent carbon (few milligrams) was placed in 10 mL of prepared solution and shaken for 24 h. The regenerated activated carbon was washed with distilled water and dried at 80 °C. The effectiveness of regeneration was evaluated by subsequent regeneration-batch adsorption cycles.

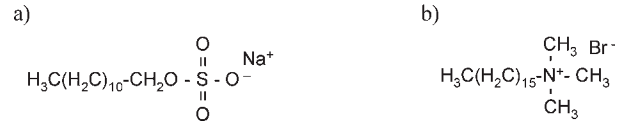

a)

$H_3C(H_2C)_{10}\text{-}CH_2O\text{-}\overset{O}{\underset{O}{S}}\text{-}O^{-}\ Na^{+}$

b)

$H_3C(H_2C)_{15}\text{-}\overset{CH_3}{\underset{CH_3}{N^{+}}}\text{-}CH_3\ Br^{-}$

Figure 2. Molecular formula of the surfactants: (a) SDS and (b) HDTA.

RESULTS AND DISCUSSION

Physical and Chemical Characteristics of Carbons. The physical and chemical properties of activated carbons are summarized in Tables 1 and 2 and reveal that the BET surface area was 45 % higher for carbon L27. The difference in the total pore volume was even higher where carbon L27 doubled that of F400. Fractional pore volumes indicate that for F400 about 50 % of pore volume was concentrated in the (0.7 to 0.1) nm diameter range, whereas L27 is characterized by high mesopore content (61 %). As a result, average pore diameter was higher for the latter, 1.8 nm compared to 1.0 nm. The surface of activated carbons is usually rich in oxygenated functional groups such as alcoholic, phenolic, and carboxylic. Results from elemental analysis suggest that these oxygen-containing structures are more abundant on the surface of F400. Acid—base titration results indicated that the content of acidic functionalities was similar for both adsorbents, whereas the surface of carbon F400 was richer in basic sites also evidenced by its higher value of pH_{PZC}. In any case, both adsorbents had an overall basic surface with pH_{PZC} values above 9.5. The ash content was also similar suggesting a comparable inorganic content. Basically, the main differences between both adsorbents were observed in the pore distribution and the surface oxygen content reflected as distinct total surface basicity.

Effect of Contact Time. The effect of contact time on MB and ARS adsorption was studied for an initial dye concentration of $3.0\ g \cdot L^{-1}$ and solution pH of 7.0. Figure 3 depicts the adsorption profile for increasing contact time at various temperatures. Batch adsorption curves are smooth and lead to saturation (i.e., equilibrium) after a contact time of (20 to 30) h. The adsorption—time profile for both the basic and the acid dye on

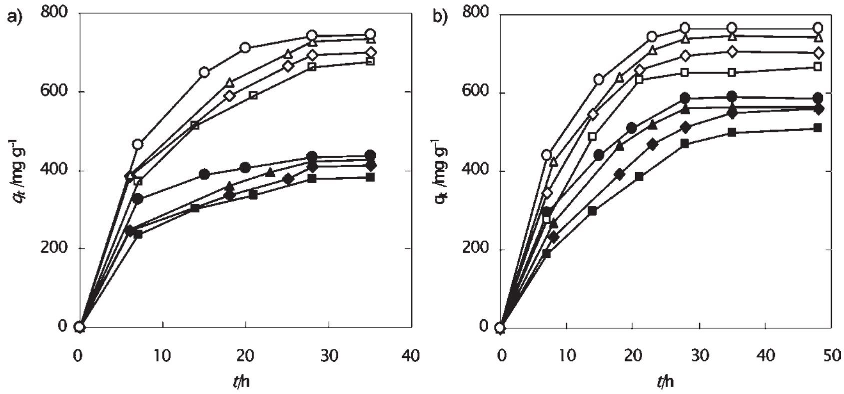

Figure 3. Effect of contact time and temperature on the adsorption of MB and ARS on F400 and L27. $C_o = 3000\ mg \cdot L^{-1}$, pH = 7. (a) MB and (b) ARS. Hollow symbols for L27 and solid symbols for F400. -■-, 15 °C; -◆-, 20 °C; -▲-, 25 °C; -●-, 30 °C.

carbon L27 was similar. Contrarily, on carbon F400 significant differences were observed depending on the solute, where the adsorption of cationic MB was less favored.

Adsorption Isotherms. Isotherm data indicate how the adsorption molecules distribute between the liquid and solid phase. Adsorption isotherms were obtained at (15, 20, 25, and 30) °C. Figure 4 shows those obtained at 15 °C, but similar results were obtained for the rest of the temperatures. The isotherms are of an L-type, indicating that the dyes have a high affinity for activated charcoal. The equilibrium data were analyzed according to the Langmuir and Freundlich isotherm models. The corresponding isotherm parameters are shown in Table 3 which indicate that these ACs have great affinity for dye adsorption. In general, correlation coefficients are close to 1.0 for both equations. However, the Langmuir equation provides the best fit for the four AC/dye systems studied in this work. The Langmuir equation assumes that a surface consists of a given number of equivalent sites where a species can physically or chemically sorb.

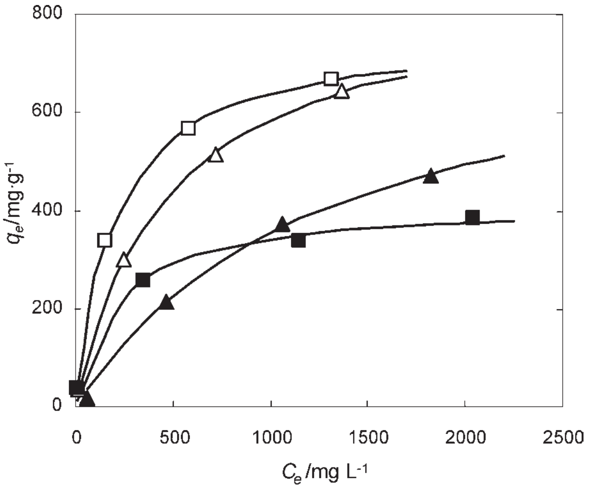

Figure 4. Isotherms of MB and ARS adsorption on F400 and L27 at 298 K. Line depicts fit to the Langmuir equation. □, L27 MB; Δ, L27 ARS; ■, F400 MB; ▲, F400 ARS.

Table 3. Isotherm Parameters of MB and ARS Adsorption on Activated Carbons L27 and F400[a]

	Langmuir				Freundlich			
	T/°C	Q	b	r^2	R_L	k_F	$1/n$	r^2
MB-L27	15	765.64	$5.0 \cdot 10^{-3}$	0.999	0.06	41.91	0.393	0.953
	20	778.10	$6.1 \cdot 10^{-3}$	0.991	0.05	45.89	0.389	0.922
	25	797.75	$8.9 \cdot 10^{-3}$	1.000	0.04	71.83	0.337	0.935
	30	796.47	$1.1 \cdot 10^{-2}$	1.000	0.03	83.74	0.320	0.931
MB-F400	15	412.53	$4.8 \cdot 10^{-3}$	0.996	0.06	39.90	0.301	0.980
	20	429.75	$6.2 \cdot 10^{-3}$	0.996	0.05	43.38	0.301	0.963
	25	454.07	$6.5 \cdot 10^{-3}$	1.000	0.05	43.42	0.310	0.941
	30	462.44	$8.7 \cdot 10^{-3}$	0.998	0.04	49.78	0.300	0.910
ARS-L27	15	855.46	$2.2 \cdot 10^{-3}$	1.000	0.13	20.07	0.485	0.988
	20	966.31	$2.0 \cdot 10^{-3}$	1.000	0.14	17.97	0.516	0.989
	25	1078.53	$1.8 \cdot 10^{-3}$	0.999	0.16	14.90	0.555	0.990
	30	1162.31	$1.7 \cdot 10^{-3}$	0.994	0.16	12.72	0.589	0.988
ARS-F400	15	808.07	$8.0 \cdot 10^{-4}$	0.998	0.29	4.21	0.633	0.981
	20	912.62	$7.0 \cdot 10^{-4}$	0.999	0.32	6.18	0.595	0.999
	25	939.8	$9.0 \cdot 10^{-4}$	0.996	0.27	7.00	0.597	0.997
	30	922.61	$1.1 \cdot 10^{-3}$	0.996	0.23	7.04	0.604	0.980

[a] Q/mg·g^{-1}; b/L·mg^{-1}.

Adsorption capacities per unit weight (Q) follow the same sequence as the pore volume of the adsorbents. Carbon L27, which is characterized by having less surface functionalities, showed the highest uptake capacity for both dyes. For all the temperatures studied, the monolayer capacity (Q) values were significantly higher for dye ARS. The highest differences between the dyes were reported for carbon F400. Furthermore, this difference increased with temperature indicating that the adsorption of the anionic dye was further favored as temperature was increased.

Considering the adsorption of dye MB, the measured monolayer adsorption capacities at 298 K were 86 % higher for carbon L27 compared to F400 (i.e., $Q = 765$ mg·g^{-1} and 412 mg·g^{-1}). However, this discrepancy was significantly lowered to about 5 % for the anionic dye ARS (i.e., $Q = 855$ mg·g^{-1} and 808 mg·g^{-1}). This behavior can be attributed to the effect of chemical properties of carbon on the adsorption mechanism. At pH 7 electrostatic attractions between the positively charged surface of ACs and the negatively charged ARS become an important driving force for the adsorption process. In this case, the less favorable textural structure of F400 was overcome by its more favorable surface chemistry (i.e., electrostatic attraction forces). It is reasonable to assume that the pore size effect becomes less relevant in adsorption when electrostatic attraction forces occur between the dye and AC surface.

A summary of some relevant published data with the adsorption properties of alternative adsorbents used for MB and ARS removal is presented in Table 4. The adsorption capacity for MB measured in this work was found to be higher than on blast furnace sludge, fly ash, or fruit peel but comparable to that on sunflower stalks, diatomite, and spent tea leaves. High adsorptive capacity for the removal of methylene blue by bentonite, despite its reduced BET surface area, has been observed by other workers. The electrical charge and hydrophilic characteristics of its surface could be responsible for such high capacities. In general, the amount adsorbed by the activated carbons used in this work is high compared with other alternative low cost sorbents reported in the literature and similar to other ACs. For example, Hameed et al.[26] reported adsorption capacities for MB onto AC prepared from rattan sawdust in the order of 300 mg·g^{-1} after 24 h contact time. Surface area and average pore size of ACs in these studies were similar to the ones measured in the present work. Other works,[27,28] although with different textural properties (i.e., BET area, total, and micropore volume) measured for F-400 also reported similar uptake capacities for MB. Reported values for MB adsorption on ACs prepared from fruit stones are much smaller and fall in the range from (1 to 9) mg·g^{-1}.[29] These latter adsorbents had significantly smaller BET surface areas, in the range of 200 m^2·g^{-1}. However, the observed differences in the uptake capacity are more likely to arise from the amount and nature of surface functionalities.

It is more scarce that works investigate adsorption of ARS onto alternative sorbents. Uptake capacities reported in this work for ACs are well above those reported for mesoporous gels or hydroxyapatite. Iqbal et al.[30] reported a Freundlich constant for ARS of about 7 mg·g^{-1} on activated charcoal. Wu et al.[31] reported a maximum monolayer capacity for adsorption of ARS on xerogels of about 30 mg·g^{-1}. The low values of pH$_{PZC}$ (i.e., 4.5 to 7.0) and the relatively smaller BET area

Table 4. Comparison of the Adsorption Capacities and Other Parameters for the Removal of Basic Dyes by Alternative Adsorbents

adsorbent	dye	S_{BET}	Q	concentration range	contact time	pH	source
this work	MB	925 to 1345	376 to 742	100 to 3000	24	7	
blast furnace sludge	MB	28	6.4	-	2	6.5 to 7.5	Jain et al.[47]
fly ash	MB	16	6.4	0.3 to 3.2	100	-	Wang et al.[48]
banana peel	MB	23	21	10 to 120	24	-	Annadurai et al.[49]
sunflower stalk	MB	1.2	205	100 to 2000	120	-	Sun and Xu[50]
diatomite	MB	33	143	45 to 640	72	-	Shawabkeh and Tutunji[51]
spent tea leaves	MB	—	300	35 to 400	3	-	Hameed[52]
bentonite	MB	28	1667	100 to 1000	3	7.9	Ozacar and Sengil[53]
this work	ARS	925 to 1345	470 to 762	100 to 3000	24	7	
hydroxyapatite	ARS	80	0.068	68	0.25	6.9	Moriguchi et al.[54]
mesoporous hybrid gels	ARS	47 to 671	20 to 34	approx. 100 to 600	144	2	Wu et al.[55]

[(400 to 600) $\text{mg}\cdot\text{g}^{-1}$] of these xerogels were identified as responsible for the limited adsorption capacity.

One particular feature of ACs is that the uptake capacity was high for both acid and basic dyes. The amphoteric and hetereogenic nature of their surface, with functional groups that confer electric charge and both hydrophilic and hydrophobic nature, favors this behavior. For example, peat is shown to be a particularly effective adsorbent for basic dyes; however, it has a lower capacity for acid dyes.[32] Chitosan has a low affinity for basic dyes, while clay minerals exhibit a strong affinity.[33] Another example of a specific adsorbent is alunite which showed high affinities for acid dyes.[34]

One interesting feature of the isotherm curves drawn in Figure 4 is that they cross each other. For carbon F400 it occurs within the concentration range studied, whereas for carbon L27 it seems to occur at a liquid phase dye concentration of about 1500 $\text{mg}\cdot\text{L}^{-1}$. That is, at low liquid phase solute concentrations the equilibrium capacity is higher for the cationic dye MB, whereas at high solute concentration it is higher for ARS. At low solute concentrations adsorption mechanisms such as hydrogen bonding and hydrophobic interactions could dominate. That would explain the higher uptake capacity for MB. On the contrary, at high solute concentrations, conditions become more favorable for electrostatic interactions, and adsorption of ARS is favored (higher q_e values). It is noted that acid/base interactions can occur through hydrogen bonding. As the intensity of the acid/base interaction increases, the hydrogen bond can turn into a strong ionic bond. It is likely that the nature of the bonds between dyes and AC depends on the solution concentration of the dye that affects the formation of polynuclear species.[35] At low solute concentration, weak acid/base interactions, only hydrogen bonds may be formed. For strong acid/base interactions, the interactions may gradually change to a chemical complexation.

pH Effect. The effect of pH was studied in the range from pH 4.0 to 11.0 and at 20 °C. The initial dye concentration was 1000 $\text{mg}\cdot\text{L}^{-1}$. Figure 5 shows the effect of pH on the equilibrium uptake of MB and ARS on carbon F400 and L27. It is known that the main influence of the pH occurs through the simultaneous modification of the surface charge of the adsorbent and the degree of ionization of the dyes. Both the hydrogen and the hydroxyl ions are adsorbed strongly and therefore can modify the adsorption kinetics and equilibrium properties of other molecules depending on the characteristics of the adsorbent—adsorbate interactions.

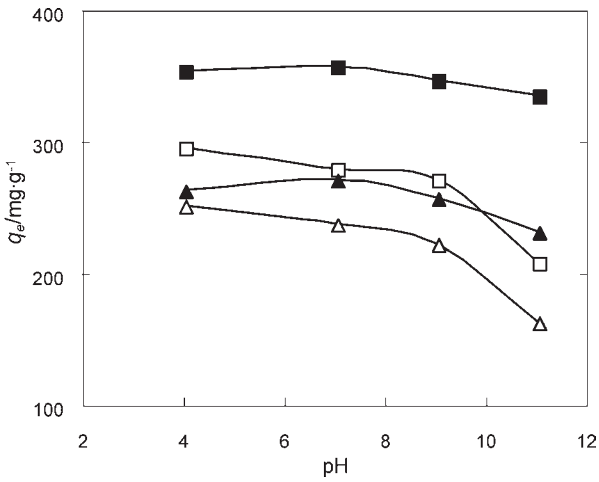

Figure 5. Effect of pH on the equilibrium adsorption of MB and ARS on activated carbon F400 and L27. $T = 20$ °C, $C_o = 1000$ $\text{mg}\cdot\text{L}^{-1}$. □, L27 ARS; △, F400 ARS; ■, L27 MB; ▲, F400 MB.

If the acid/base interaction is the main adsorption mechanism, adsorption will depend on the valence states and therefore also on the pH of the solution. Figure 5 shows that adsorption of ARS onto both ACs was pH-dependent, supporting the acid/base interaction. Alizarin red S is negatively charged at pH values above 4.5, and the adsorption of ARS can occur by interaction with the positively charged sites on the surface of activated carbon. For the cationic dye (MB), no significant influence of pH on the adsorption capacity was observed onto any of the two activated carbons. There is a slight decrease with the increase of the pH. In water at pH < 12 methylene blue is positively charged since the pK_a is greater than 12 and the condition becomes unfavorable for dye uptake by electrostatic interaction. However, MB is readily adsorbed onto the predominantly positive surface of AC. Similar results were also reported by others. The sorption of MB remained almost unchanged onto oxihumolite at about 50 $\text{mg}\cdot\text{g}^{-1}$ (initial concentration 1000 $\text{mg-MB}\cdot\text{L}^{-1}$) in the 1 to 5 pH range.[36] Garg et al.[37] observed a similar behavior when studying adsorption onto saw dust. The sorption of acid dyes, on the other hand, was affected more strongly by the pH change.

There are double bonds and benzene rings in the dye molecules, and they are all hydrophobic structures. The observed behavior suggests that adsorption of MB is likely to occur through hydrophobic interaction rather than electrostatic interaction. The former generate weaker binding interactions that would explain the lower activation energy values reported for MB in comparison to ARS which will be further discussed in the Thermodynamic Study section.

At pH < pH_{PZC}, MB and ARS were readily adsorbed on the amphoteric surface of the activated carbons. As the pH approaches 11.5 (pH > pH_{PZC}), ARS gains another negative charge, and negatively charged functionalities increase on the surface. As a consequence, the electrostatic repulsion is predominant, and the adsorption of negatively charged ARS is significantly hindered.

Within the whole pH range studied, from pH 4.0 to 11.0, equilibrium uptake capacities for MB were higher than those measured for ARS. Differences in q_e ranged from 20 % to 60 % and increased with the pH. This suggests that the dual mechanism of adsorption, associated to the fact that isotherms crossed each other, occurs within all the pH ranges expected in wastewater. The occurrence of two parallel adsorption mechanisms, one involving electrostatic interactions and a second one involving dispersive interactions, was also proposed by others.[38]

Kinetic Modeling. To investigate the adsorption process, the sorption data were analyzed using three kinetic models, including the pseudo-first-order (PFO), pseud-osecond-order (PSO), and intraparticle diffusion (IPD) model. These represent apparent kinetics which is in fact a result of combined mechanisms. However, the obtained parameters can serve to ascertain the predominant mechanism, to predict the rate at which contamination is removed from aqueous solutions, and also as a means for studying the effect of adsorbent and adsorbate properties. The PFO model is explained as follows

$$\frac{dq}{dt} = k_1(q_e - q_t) \tag{6}$$

After integration and rearrangement, eq 6 becomes

$$q_t = q_e(1 - \exp(-k_1 t)) \tag{7}$$

where q_e and q_t are amounts of dye adsorbed ($\text{mg}\cdot\text{g}^{-1}$) at equilibrium and time t (h), respectively, and k_1 is the rate constant of the pseudo-first-order adsorption (1/h).

The PSO kinetic model is explained as follows

$$\frac{dq}{dt} = k_2(q_e - q_t)^2 \tag{8}$$

The integrated and rearranged form of eq 8 becomes

$$q_t = \frac{k_2 q_e^2}{1 + k_2 q_e t} \tag{9}$$

where k_2 is the rate constant of pseudo-second-order adsorption ($\text{g}\cdot\text{mg}^{-1}\cdot\text{h}^{-1}$). Nonlinear regression by the least-squares error method was used to fit experimental data to the PFO and PSO models since it proved to give a better estimation of equilibrium uptake capacities compared to linear regression.

The possibility of intraparticular diffusion is explored by using the following equation

$$q_t = k_d t^{0.5} + C \tag{10}$$

where C is the intercept and k_d ($\text{mg}\cdot\text{g}^{-1}\cdot\text{h}^{-0.5}$) is the intraparticle diffusion rate constant. These were calculated by linear regression. The values of intercept C provide information about the steps involved in the adsorption process. If C is equal to zero, the only controlling step is intraparticle diffusion. If $C \neq 0$, the adsorption process is rather complex and involves more than one diffusive resistance thickness. For example, the higher the intercept is, the higher the external resistance to mass transfer.

The best fitting parameter values and statistical parameters are summarized in Table 5. From them it is observed that the PFO and PSO models achieved similar overall values for the root-mean-square error (RMSE), defined as in eq 11, and the coefficients of determination, r^2. Thus, both models adequately represent off-equilibrium sorption for the studied system. Other works[39,40] reported that the PSO equation usually better describes the kinetics of adsorption of dyes onto porous media.

Table 5. Kinetic Parameters for MB and ARS Adsorption onto Activated Carbon L27 and F400[a,b]

			pseudo-first-order				pseudo-second-order				intraparticle diffusion			activation energy	
	T	$q_{e,\text{exp}}$	k_1	$q_{e,\text{est}}$	rmse	r^2	k_2	$q_{e,\text{est}}$	rmse	r^2	K_d	C	r^2	K_o	E_A
MB-L27	15	674.00	$1.05\cdot10^{-1}$	681.24	15.7	0.981	$9.70\cdot10^{-5}$	920.59	10.3	0.995	109.36	88.82	0.993	5.93	9.58
	20	692.52	$1.26\cdot10^{-1}$	693.02	20.2	0.974	$1.31\cdot10^{-4}$	888.46	12.7	0.993	109.70	116.77	0.999		
	25	727.20	$1.18\cdot10^{-1}$	736.85	16.8	0.985	$1.17\cdot10^{-4}$	945.58	8.4	0.997	120.55	96.79	0.996		
	30	742.08	$1.34\cdot10^{-1}$	758.15	5.3	0.998	$1.64\cdot10^{-4}$	925.00	9.1	0.994	135.89	109.19	0.993		
MB-F400	15	376.05	$1.32\cdot10^{-1}$	371.73	11.5	0.955	$3.88\cdot10^{-4}$	432.30	11.1	0.988	52.65	98.46	0.993	316.33	18.68
	20	408.94	$1.53\cdot10^{-1}$	389.87	19.7	0.902	$3.30\cdot10^{-4}$	470.09	17.0	0.950	55.61	105.70	0.990		
	25	423.53	$1.47\cdot10^{-1}$	412.58	14.7	0.952	$2.20\cdot10^{-4}$	544.08	13.0	0.987	61.16	101.61	1.000		
	30	434.63	$2.05\cdot10^{-1}$	420.22	11.6	0.916	$5.01\cdot10^{-4}$	494.35	7.4	0.987	40.73	222.77	0.989		
ARS-L27	15	652.44	$6.64\cdot10^{-2}$	798.87	22.0	0.980	$4.02\cdot10^{-5}$	1186.59	26.3	0.970	184.34	−208.55	0.999	1430.10	23.79
	20	693.32	$8.81\cdot10^{-2}$	767.12	8.0	0.997	$7.74\cdot10^{-5}$	1023.24	15.0	0.990	161.84	−74.99	0.993		
	25	738.10	$9.51\cdot10^{-2}$	792.09	6.3	0.997	$8.15\cdot10^{-5}$	1053.71	5.7	0.998	144.79	18.72	0.999		
	30	762.31	$1.12\cdot10^{-1}$	795.83	9.0	0.995	$1.10\cdot10^{-4}$	1023.00	37.4	0.996	140.69	73.99	0.994		
ARS-F400	15	469.49	$4.73\cdot10^{-2}$	627.95	10.0	0.992	$2.92\cdot10^{-5}$	1021.59	8.7	0.995	104.74	−90.10	0.998	4563.75	27.67
	20	514.10	$5.11\cdot10^{-2}$	673.10	6.9	0.996	$2.04\cdot10^{-5}$	1268.89	13.0	0.998	115.95	−94.79	0.998		
	25	560.05	$6.52\cdot10^{-2}$	669.50	2.2	1.000	$4.63\cdot10^{-5}$	1003.07	5.9	0.997	120.23	−61.96	0.988		
	30	583.91	$8.25\cdot10^{-2}$	637.56	12.0	0.989	$7.28\cdot10^{-5}$	899.41	7.2	0.997	110.20	7.83	0.997		

[a] C_o = 3000 $\text{mg}\cdot\text{L}^{-1}$, pH = 7.0, m_{GAC} = 25 mg, solute to sorbent mass ratio is 1200 $\text{mg}\cdot\text{g}^{-1}$ (T/°C; $q_{e,\text{exp}}/\text{mg}\cdot\text{g}^{-1}$; k_1/h^{-1}; $q_{e,\text{est}}/\text{mg}\cdot\text{g}^{-1}$; $k_2/\text{g}(\text{mg}\cdot\text{h})^{-1}$; $K_d/\text{mg}\cdot\text{g}^{-1}\cdot\text{min}^{-0.5}$; K_o/h^{-1}; $E_A/\text{kJ}\cdot\text{mol}^{-1}$). [b] Activation energy measured using k_1 as the kinetic constant.

Plazinski et al.[41] have recently published a review of a certain class of theoretical models describing the kinetics of pollutant sorption onto various sorbents. They suggest that when a significant part of data are collected when the system is not very close to equilibrium the PFO model can better describe sorption. Furthermore, the commonly accepted procedure of treating q_e as a best-fit parameter leads to the best correlation of data by a pseudo-first-order model. In the present work, we have observed that the equilibrium uptake capacities, q_e, estimated by these models significantly differ from each other. The values for q_e estimated by the PFO model are in better agreement with the experimental data ($q_{e,exp}$) presented in Table 5. The pseudo-first-order equation is only an approximate solution of other more complicated rate mechanisms. However, due to its simplicity and its adequate fitting in the present adsorption system, the determination of activation energy (E_A) was done by using the values of k_1 as the kinetic constant.

$$\text{rmse} = \sqrt{\frac{\sum_{i=0}^{i=n} (q_{\exp} - q_{\text{est}})^2}{n}} \tag{11}$$

From the results in Table 5 it is observed that the C values for the boundary layer increase with the temperature, especially for ARS. This is due to fact that with the rise in temperature the mobility of ions increases, which decreases the retarding force acting on the diffusing ions. This suggests the involvement of film diffusion at high temperatures and particle diffusion mechanisms at lower temperatures, as the rate-controlling steps.

The apparent kinetic constant k_1 represents the fractional uptake for a given contact time, and as expected, higher values were measured for MB since it has the lower q_e. The paired samples t test was used to test for a difference between k_1 and q_e values shown in Table 5. Results from the t test shown in Table 6 revealed statistically significant difference (t test $p < 0.05$) between k_1 and q_e values measured for both dyes onto a given AC (pairs 1−2 and pair 6) and between both ACs for a given dye (pairs 3−4 and pairs 7−8). The only nonsignificant difference occurred for pair 5 ($p = 0.465$) that indicates that equilibrium uptake q_e onto L27 was independent of the solute electric charge. Thus, for the carbon with less surface basicity, L27, no significant correlation could be established between the acidity/basicity of the dye and the color removal. The higher adsorption rate for MB (pair 1) suggests that transport of the cationic dye MB from bulk solution to the surface was more favorable than for the anionic dye ARS.

Table 6. *t* Test for Mean Comparison between Paired Samples

		mean	N	standard deviation	mean difference	t test sig.
pair 1	$k_{1,\text{MB-L27}}$	0.121	4	0.012		
	$k_{1,\text{ARS-L27}}$	0.090	4	0.019	0.030	0.007
pair 2	$k_{1,\text{MB-F400}}$	0.160	4	0.031		
	$k_{1,\text{ARS-F400}}$	0.061	4	0.016	0.098	0.002
pair 3	$k_{1,\text{MB-L27}}$	0.121	4	0.012		
	$k_{1,\text{MB-F400}}$	0.160	4	0.032	−0.038	0.038
pair 4	$k_{1,\text{ARS-L27}}$	0.090	4	0.019		
	$k_{1,\text{ARS-F400}}$	0.061	4	0.016	0.029	0.004
pair 5	$q_{e,\text{MB-L27}}$	706.1	4	35.7		
	$q_{e,\text{ARS-L27}}$	711.5	4	48.7	−5.4	0.465
pair 6	$q_{e,\text{MB-F400}}$	410.7	4	25.4		
	$q_{e,\text{ARS-F400}}$	531.9	4	50.7	−121.1	0.003
pair 7	$q_{e,\text{MB-L27}}$	706.1	4	35.7		
	$q_{e,\text{MB-F400}}$	410.7	4	25.4	295.3	<0.001
pair 8	$q_{e,\text{ARS-L27}}$	711.5	4	48.7		
	$q_{e,\text{ARS-F400}}$	531.9	4	50.7	179.7	<0.001

Activation Energy. For the basic dye MB, values of E_A varied significantly between sorbents from (9.6 to 18.7) kJ·mol^{-1} (Table 5). Arrhenius plots are drawn in Figure 6. For the anionic dye, ARS similar values of E_A, in the range of (23.8 to 27.7) kJ·mol^{-1}, were measured for both sorbents. The physisorption process normally has an activation energy of (5 to 40) kJ·mol^{-1}, while chemisorption has a higher activation energy of (40 to 800) kJ·mol^{-1}.[42] The values reported in this work indicate that adsorption is mainly controlled by a physical process since the temperature dependence of diffusivity is relatively weak.

The highest E_A values were measured, among the solutes, for the acid dye ARS and, among the sorbents, for the more basic and microporous carbon F400. As a consequence, the maximum value was reported for the adsorption of ARS on F400 that suggests that the mechanism of adsorption involves ionic interactions. The lower values measured for MB support results from the previous section in that weak adsorption forces such as van der Waals are involved in the adsorption of the cationic solute. These values are below, though in the same order of magnitude of, other activation energies of adsorption reported in the literature which varied in the range from (33.35 to 47.5) kJ·mol^{-1} for the adsorption of dyes onto sorbents such as sepiolite,[43] carbon nanotubes,[42] or silk.[44]

An increase in temperature leads to an increase in equilibrium dye uptake (see Tables 3 and 5). This effect is more marked within the (15 to 25) °C temperature range. Other works reported an opposite trend where the increase in temperature leads to a decrease in MB adsorption onto water-hyacinth[45] and on clay.[35] These were obtained within a wider temperature range, up to 60 °C. This behavior was attributed to the formation at lower temperatures of high charge polymeric species responsible for more intense electrostatic interactions. The monomeric form becomes dominant at higher temperatures, and therefore

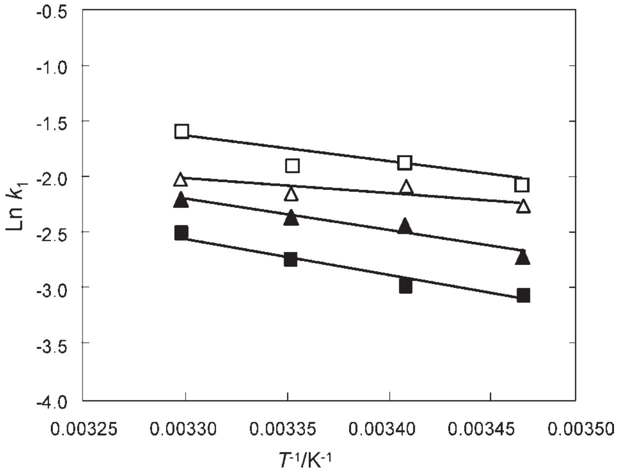

Figure 6. Plots of ln(k_1) versus $1/T$ for adsorption of dyes ARS and MB on activated carbons F400 and L27. □, F400 MB; Δ, L27 MB; ■, F400 ARS; ▲, L27 ARS.

Table 7. Thermodynamic Parameters for the Adsorption of MB and ARS on Activated Carbons L27 and F400[a]

	T	thermodynamic equilibrium constant (K_c)	$\Delta G°$	$\Delta S°$	$\Delta H°$
MB-L27	15	3.83			
	20	7.00			
	25	7.10	−4.86	137.5	36.1
	30	8.76			
MB-F400	15	1.98			
	20	2.66			
	25	2.95	−2.68	118.1	32.4
	30	4.02			
ARS-L27	15	1.88			
	20	1.93			
	25	1.94	−1.64	12.9	2.2
	30	1.98			
ARS-F400	15	0.65			
	20	0.64			
	25	0.85	0.41	78.4	23.8
	30	1.01			

[a] T/°C; $\Delta G°$/kJ·mol^{-1}; $\Delta S°$/J·(mol·K)$^{-1}$; $\Delta H°$/kJ·mol^{-1}.

adsorption of water molecules by dipole−dipole interactions dominates.

Thermodynamic Study. To fully understand the nature of adsorption, the thermodynamic studies play an important role. Thermodynamic parameters related to the adsorption of dyes such as Gibbs energy change ($\Delta G°$), enthalpy change ($\Delta H°$), and entropy change ($\Delta S°$) are presented in Table 7. Due to the physical meaning attributed to its constants, $Q \cdot b$ was used for the determination of the thermodynamic parameters.

The values of Gibbs energy are negative indicating that the process is spontaneous except for the F400-ARS system. The high activation energy required for this system could be responsible. The positive $\Delta S°$ values reflect the affinity of the adsorbent materials toward dyes. The positive values of enthalpy change indicate the endothermic nature of adsorption, as was noted when the effect of temperature was studied. This may suggest that the pore size of the adsorbents is relatively small compared to the molecular size of the dyes and that intraparticle transport was limiting the adsorption. Also the enthalpy change values indicate that adsorption of the anionic dye is thermodynamically more favorable onto L27 than F400. The cationic dye has similar $\Delta G°$ and $\Delta H°$ values for both activated carbons.

Desorption. Regeneration of spent activated carbon was done using different solutions. A basic solution (0.1 M NaOH) was used since favorable desorption was reported in previous work.[46] The regeneration ability of two additional solutions containing either anionic surfactant SDS or cationic HDTA was also evaluated. Results in Figure 7 show little desorption of MB from both adsorbents by using a 0.1 M NaOH solution. MB was bound through hydrophobic interactions, and modification of solution pH did not allow dye desorption (regenerability below 9 %). For the anionic dye ARS, after three cycles, the regeneration was 24 % and 17 % for L27 and F400, respectively. At high pH values the negatively charged −OH and $-SO_3$ groups of ARS and the adsorbent surface generate repulsive interactions that would explain the higher reversibility.

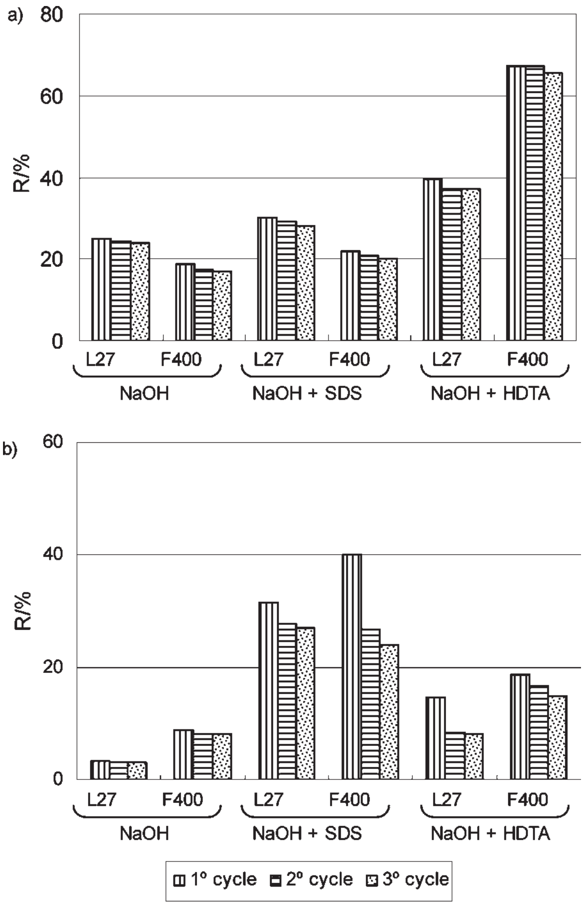

Figure 7. Percent uptake capacity, with respect to the first use, for subsequent adsorption cycles using as regeneration solutions: 0.1 M NaOH; 0.1 M NaOH + SDS; and NaOH + HDTA. (a) ARS and (b) MB.

Surfactant molecules are amphiphilic in nature having a hydrophilic (head) and hydrophobic (tail) part (Figure 2). The use of surfactants above the CMC showed to modify the desorption abilities of all the dye-activated carbon systems. For the cationic dye, MB regeneration ability is significantly enhanced for both activated carbons. The best performance was observed for the anionic surfactants SDS. During desorption (pH > 10) micelles of SDS are negatively charged and therefore are unlikely to be adsorbed onto negatively charged surface of activated carbons. On the other hand, due to strong hydrophobic interactions between the adsorbed MB and the micellar core, dye gets solubilized in the micelle. Consequently, desorption of dye MB is enhanced for both F400 and L27 activated carbons.

For the anionic dye ARS a different behavior was observed. SDS hardly increased desorption. However, the adsorbed ARS solute readily desorbs and binds to micelles of HDTA. This behavior was observed for both activated carbons, but it was more pronounced in the case of F400. Ionic pollutants having opposite charge to that of the micellar surface can be bound on its outer periphery where the the valence state is higher, and therefore, the binding is greater.

The obtained results suggest that for adequate desorption it is more important to enhance interaction between dye and surfactant rather than the repulsion between micelles and adsorbent surface. This is inferred from the enhanced desorption of the anionic dye ARS by the cationic surfactant (HDTA), whereas the anionic surfactant (SDS) better performs for the desorption of the cationic dye MB. The surfactant-enhanced desorption was more effective for the more oxygen-containing surface carbon F400. For both the cationic and anionic dye, maximum regeneration was achieved for this adsorbent with values between (67 to 65) % and (40 to 24) % for the three subsequent cycles.

It is noteworthy that the reversibility of each adsorption system follows the same order as the E_A. The best regeneration performance was reported for ARS-F400 which had also the highest activation energy followed by ARS-L27 which is precisely the system with the second highest activation energy. The main driving force of physical adsorption is electrostatic attraction and van der Waals force. In the kinetic study section, we concluded that electrostatic interaction was involved in the adsorption mechanism of the anionic dye. Results from the regeneration study suggest that reversibility is favored when adsorption involves electrostatic interactions.

The use of surfactants has an evident environmental advantage compared to other regeneration methods such as physical regeneration by steam or chemical regeneration by organic solvents. However, at the selected conditions in the present work only moderate regeneration of these activated carbons was achieved. More severe conditions by modification of NaOH concentration or ionic strength should be evaluated.

CONCLUSIONS

The present research work focuses on the effect of the structural properties of the adsorbent in the adsorption of industrial dyes. Synthetic dyes MB and ARS and the activated carbons F400 and L27, with different pore distribution and surface oxygen content, were used for the study. Thermodynamic properties were measured and related to adsorption performance.

From the physicochemical analysis, the carbon L27 was the more mesoporous and with less surface basicity. Also, it was concluded that low basicity is a key factor since it allows favorable adsorption of both acid and basic dyes.

Higher correlation coefficients indicate that the Langmuir isotherm fit the adsorption data better than the Freundlich isotherm. Adsorption capacities per unit weight (Q) follow the same sequence as the surface area of the adsorbents. However, it was strongly affected by chemical properties which affected the adsorption mechanism. It was concluded that the pore size effect becomes less relevant in adsorption when electrostatic attraction forces occur between the dye and AC surface.

The maximum amount adsorbed, at the lowest temperature of 15 °C, was 765.6 $\text{mg}\cdot\text{g}^{-1}$ and 855.45 $\text{mg}\cdot\text{g}^{-1}$ for MB and ARS, respectively. These are high compared with other sorbents reported in the literature. Adsorption kinetics and equilibrium properties of the basic dye were more dependent on AC properties compared to the acid dye. This trend can be attributed to differences in the adsorption mechanism. Hydrophobic interaction plays a dominant role in the adsorption of the cationic dye, whereas the anionic dye was bound through electrostatic interaction. This coincides with the lower activation energy values reported for MB [(9.58 to 18.68) $\text{kJ}\cdot\text{mol}^{-1}$] in comparison to ARS [(23.79 to 27.67) $\text{kJ}\cdot\text{mol}^{-1}$]. It is likely that the nature of the bonds between dyes and AC depends on the solution concentration of the dye that affects the formation of polynuclear species.

The adsorption processes of cationic and anionic dyes on ACs studied obey the pseudo-first-order model. The highest difference in k_1 was reported among dyes in the adsorption onto carbon F400. The highest difference in q_e was reported among sorbents, for adsorption of dye MB.

The equilibrium adsorption capacity for both dyes increased with temperature, and the reactions were endothermic. The enthalpy change was the highest (positive) for basic dye adsorption.

For adequate desorption it is more important to enhance interaction between dye and surfactant rather than the repulsion between micelles and adsorbent surface. This is inferred from the enhanced desorption of the anionic dye ARS by cationic surfactant (HDTA), whereas the anionic surfactant (SDS) better performs for the desorption of the cationic dye MB.

It is noteworthy that the regenerability of each adsorption system follows the same order as the E_A. The best regeneration performance was reported for ARS-F400 which also had the highest activation energy followed by ARS-L27 which is precisely the system with the second highest activation energy.

AUTHOR INFORMATION

Corresponding Author

*Phone: +34-94 501 30 30. Fax: +34-94 601 59 63. E-mail: unai.iriarte@ehu.es.

Funding Sources

The authors wish to thank to the Universidad del País Vasco, the Ministerio de Educación Cultura y Deporte (grant AP 99 30687378), the Departamento de Industria, Comercio y Turismo (project OD03UN57), and the water engineering firms Pridesa and Cetolar for their technical and economic support.

REFERENCES

(1) Oakes, J.; Gratton, P. Kinetic investigations of the oxidation of arylazonaphthol dyes in hypochlorite solutions as a function of pH. *J. Chem. Soc., Perkin Trans.* **1998**, *2*, 2201–2206.

(2) Lin, S. H.; Lo, C. C. Treatment of textile wastewater by foam flotation. *Environ. Technol.* **1996**, *17*, 841–849.

(3) Lopez-Grimau, V.; Gutierrez, M. C. Decolourisation of simulated reactive dyebath effluents by electrochemical oxidation assisted by UV light. *Chemosphere* **2006**, *62*, 106–112.

(4) Mohorcic, M.; Teodorovic, S.; Golob, V.; Friedrich, J. Fungal and enzymatic decolourisation of artificial textile dye baths. *Chemosphere* **2006**, *63*, 1709–1717.

(5) Kapdan, I. K.; Ozturk, R. Effect of Operating Parameters on Color and COD Removal Performance of SBR, Sludge Age and Initial Dyestuff Concentration. *J. Hazard. Mater.* **2005**, *123*, 217–222.

(6) Golob, V.; Vinder, A.; Simonič, M. Efficiency of the coagulation/flocculation method for the treatment of dyebath effluents. *Dyes Pigm.* **2005**, *67*, 93–97.

(7) Chen, J. X.; Zhu, L. H. Catalytic degradation of Orange II by UVFenton with hydroxyl-Fe-pillared bentonite in water. *Chemosphere* **2006**, *65*, 1249–1255.

(8) Dasneshvar, N.; Aloboyeh, A.; Khataee, A. R. The evaluation of electrical energy per order for photooxidative decolorization of four textile dye solutions by the kinetic model. *Chemosphere* **2005**, *59*, 761–717.

(9) Crini, G. Non-conventional low-cost adsorbents for dye removal: A review. *Bioresour. Technol.* **2006**, *97*, 1061–1085.

(10) Dabrowski, A. Adsorption, from theory to practice. *Adv. Colloid Interface Sci.* **2001**, *93*, 135–224.

(11) Dogan, M.; Alkan, M. Adsorption kinetics of methyl violet onto perlite. *Chemosphere* **2003**, *50*, 517–528.

(12) Bereket, G.; Arogus, A. Z.; Ozel, M. Z. Removal of Pb(II), Cd(II), Cu(II) and Zn(II) from aqueous solutions by adsorption on bentonite. *J. Colloid Interface Sci.* **1997**, *187*, 338–343.

(13) Mohamed, M. M. Adsorption properties of ionic surfactants on molybdenum-modified silica gels. *Colloid Surf., A* **1996**, *108*, 39–48.

(14) Mohan, D.; Singh, K. P.; Kumar, K. Removal of dyes from wastewater using fly ash, a low cost adsorbent. *Ind. Eng. Chem. Res.* **2003**, *42*, 1965–1976.

(15) Allen, S. J.; Mckay, G.; Khader, K. Y. H. Equilibrium adsorption isotherms for basic dyes onto lignite. *J. Chem. Technol. Biotechnol.* **1989**, *45*, 291–302.

(16) Ho, Y. S.; Mckay, G. Sorption of dye from aqueous solution by peat. *Chem. Eng. J.* **1998**, *70*, 115–124.

(17) Mckay, G.; Otterburn, M. S.; Sweeney, A. G. Surface mass transfer processes during colour removal from effluent using silica. *Water Res.* **1981**, *15*, 327–331.

(18) Pendleton, P.; Wu, S. H. Kinetics of dodecanoic acid adsorption from caustic solution by activated carbon. *J. Colloid Interface Sci.* **2003**, *226*, 245–250.

(19) Tsai, W. T.; Chang, C. Y.; Lin, M. C.; Chien, S. F.; Sun, H. F.; Hsieh, M. F. Adsorption of acid dyes onto activated carbon prepared from agricultural waste bagasse by $ZnCl_2$ activation. *Chemosphere* **2001**, *45*, 51–58.

(20) Kadirvelu, K.; Karthika, C.; Vennilamani, N.; Pattabhi, S. Activated carbon from industrial solid waste as an adsorbent for the removal of Rhodamine-B from aqueous solution: kinetic and equilibrium studies. *Chemosphere* **2005**, *60*, 1009–1017.

(21) Le Cloirec, P.; Faur, C. Adsorption of organic compounds onto activated carbon-application in water and air treatments. In *Activated carbon surfaces in environmental remediation*; Bandosz, T. J., Eds.; New York: Academic Press, 2006; pp 375−419.

(22) Rafatullah, M.; Sulaiman, O.; Hashim, R.; Ahmad, A. Adsorption of methylene blue on low-cost adsorbents: A review. *J. Hazard. Mater.* **2010**, *177*, 70–80.

(23) Boehm, H. P. Some aspects of the surface chemistry of carbon blacks and other carbons. *Carbon* **1994**, *32*, 759–769.

(24) Khezami, L.; Capart, R. Removal of chromium(VI) from aqueous solution by activated carbons: Kinetic and equilibrium studies. *J. Hazard. Mater.* **2005**, *123*, 223–231.

(25) Purkait, M. K.; DasGupta, S. Adsorption of eosin dye on activated carbon and its surfactant based desorption. *J. Environ. Manage.* **2005**, *76*, 135–142.

(26) Hameed, B. H.; Ahmad, A. L.; Latiff, K. N. A. Adsorption of basic dye (methylene blue) onto activated carbon prepared from rattan sawdust. *Dyes Pigm.* **2007**, *75*, 143–149.

(27) Liu, M. Y.; Tsang, D. C. W.; Hu, J.; Ng, K. T. W.; Liu, T.; Lo, I. M. C. Adsorption of Methylene Blue and Phenol by Wood Waste Derived Activated Carbon. *J. Environ. Eng.* **2008**, *134*, 338–345.

(28) El Qada, E. N.; Allen, S. J.; Walker, G. M. Adsorption of basic dyes from aqueous solution onto activated carbons. *Chem. Eng. J.* **2008**, *135*, 174–184.

(29) Aygun, A.; Yenisoy-Karakas, X. S.; Duman, I. Production of granular activated carbon from fruit stones and nutshells and evaluation of their physical, chemical and adsorption properties. *Microporous Mesoporous Mater.* **2003**, *66*, 189–195.

(30) Iqbal, M. J.; Ashiq, M. N. Adsorption of dyes from aqueous solutions on activated charcoal. *J. Hazard. Mater.* **2007**, *139*, 57–66.

(31) Wu, Z.; Ahn, I. S.; Lee, C. H.; Kim, J. H.; Shul, Y. G.; Lee, K. Enhancing the organic dye adsorption on porous xerogels. *Colloids Surf. A* **2004**, *240*, 157–164.

(32) Allen, S. J.; McKay, G.; Porter, J. F. Adsorption isotherm models for basic dye adsorption by peat in single and binary component systems. *J. Colloid Interface Sci.* **2004**, *280*, 322–333.

(33) Bagane, M.; Guiza, S. Removal of a dye from textile effluents by adsorption. *Ann. Chim. Sci. Mater.* **2000**, *25*, 615–626.

(34) Özacar, M.; Sengil, A. I. Adsorption of acid dyes from aqueous solutions by calcined alunite and granular activated carbon. *Adsorption* **2002**, *8*, 301–308.

(35) Gürses, A.; Doğar, Ç.; Yalçın, M.; Açıkyıldız, M.; Bayrak, R.; Karaca, S. The adsorption kinetics of the cationic dye, methylene blue, onto clay. *J. Hazard. Mater.* **2006**, *131*, 217–228.

(36) Janoš, P.; Šedivý, P.; Rýznarová, M.; Grötschelová, S. Sorption of basic and acid dyes from aqueous solutions onto oxihumolite. *Chemosphere* **2005**, *59*, 881–886.

(37) Garg, V. K.; Amita, M.; Kumar, R.; Gupta, R. Basic dye (methylene blue) removal from simulated wastewater by adsorption using Indian Rosewood sawdust: a timber industry waste. *Dyes Pigm.* **2004**, *63*, 243–250.

(38) Radovic, L. R.; Silva, I. F.; Ume, J. I.; Menendez, J. A.; Leon y Leon, C. A.; Scaroni, A. W. An experimental and theoretical study of the adsorption of aromatics possessing electron-withdrawing and electron-donating functional groups by chemically modified activated carbons. *Carbon* **1997**, *35*, 1339–1348.

(39) Faria, P. C. C.; Orfao, J. J. M.; Pereira, M. F. R. Adsorption of anionic and cationic dyes on activated carbons with different surface chemistries. *Water Res.* **2004**, *38*, 2043–2052.

(40) Rodríguez, A.; García, J.; Ovejero, G.; Mestanza, M. Adsorption of anionic and cationic dyes on activated carbon from aqueous solutions: Equilibrium and kinetics. *J. Hazard. Mater.* **2009**, *172*, 1311–1320.

(41) Plazinski, W.; Rudzinski, W.; Plazinska, A. Theoretical models of sorption kinetics including a surface reaction mechanism:A review. *Adv. Colloid Interface Sci.* **2009**, *152*, 2–13.

(42) Wu, C. H. Adsorption of reactive dye onto carbon nanotubes: equilibrium, kinetics and thermodynamics. *J. Hazard. Mater.* **2007**, *144*, 93–100.

(43) Dogan, M.; Alkan, M.; Demirbas, O.; Ozdemir, Y.; Ozmetin, C. Adsorption kinetics of Maxilon Blue GRL onto sepiolite from aqueous solutions. *Chem. Eng. J.* **2006**, *124*, 89–101.

(44) Önal, Y.; Akmil-Başar, C.; Eren, D.; Sarıcı-Özdemir, Ç.; Depci, T. Adsorption kinetics of malachite green onto activated carbon prepared from tunçbilek lignite. *J. Hazard. Mater.* **2006**, *128*, 150–157.

(45) El-Khaiary, M. I. Kinetics and mechanism of adsorption of methylene blue from aqueous solution by nitric-acid treated water-hyacinth. *J. Hazard. Mater.* **2007**, *147*, 28–36.

(46) Li, Q.; Yue, Q. Y.; Su, Y.; Gao, B. Y.; Li, J. Two-step kinetic study on the adsorption and desorption of reactive dyes at cationic polymer/bentonite. *J. Hazard. Mater.* **2009**, *165*, 1170–1178.

(47) Jain, A. K.; Gupta, V. K.; Bhatnagar, A.; Jain, S.; Suhas A comparative assessment of adsorbents prepared from industrial wastes for the removal of cationic dye. *J. Indian Chem. Soc.* **2003**, *80*, 267–270.

(48) Wang, S.; Li, L.; Wu, H.; Zhu, Z. H. Unburned carbon as a low-cost adsorbent for treatment of methylene blue-containing wastewater. *J. Colloid Interface Sci.* **2005**, *292*, 336–343.

(49) Annadurai, G.; Juang, R. S.; Lee, D. J. Use of cellulose-based wastes for adsorption of dyes from aqueous solutions. *J. Hazard. Mater.* **2002**, *92*, 263–274.

(50) Sun, G.; Xu, X. Sunflower stalk as adsorbents for color removal from textile wastewater. *Ind. Eng. Chem. Res.* **1997**, *36*, 808–812.

(51) Shawabkeh, R. A.; Tutunji, M. F. Experimental study and modeling of basic dye sorption by diatomaceous clay. *Appl. Clay Sci.* **2003**, *24*, 111–120.

(52) Hameed, B. H. Removal of cationic dye from aqueous solution using jackfruit peel as non-conventional low-cost adsorbent. *J. Hazard. Mater.* **2009**, *162*, 344–350.

(53) Ozacar, M.; Sengil, I. A. A two stage batch adsorber design for methylene blue removal to minimize contact time. *J. Environ. Manage.* **2006**, *80*, 372–379.

(54) Moriguchi, T.; Yano, K.; Nakagawa, S.; Kaji, F. Elucidation of adsorption mechanism of bone-staining agent alizarin red S on hydroxyapatite by FT-IR microspectroscopy. *J. Colloid Interface Sci.* **2003**, *260*, 19–25.

(55) Wu, Z.; Joo, H.; Ahn, I. S.; Haam, S.; Kim, J. H.; Lee, K. Organic dye adsorption on mesoporous hybrid gels. *Chem. Eng. J.* **2004**, *102*, 277–282.